Towards long lasting zirconia-based composites for dental implants. Part I: Innovative synthesis, microstructural characterization and in vitro stability

ARTICLE *in* BIOMATERIALS · MAY 2015

Impact Factor: 8.56 · DOI: 10.1016/j.biomaterials.2015.01.018

6 AUTHORS, INCLUDING:

Paola Palmero
Politecnico di Torino
57 PUBLICATIONS **339** CITATIONS
SEE PROFILE

Laura Montanaro
Politecnico di Torino
126 PUBLICATIONS **1,191** CITATIONS
SEE PROFILE

Helen Reveron
Institut National des Sciences Appliquées d…
14 PUBLICATIONS **89** CITATIONS
SEE PROFILE

Jérôme Chevalier
Institut National des Sciences Appliquées d…
184 PUBLICATIONS **3,382** CITATIONS
SEE PROFILE

Biomaterials 50 (2015) 38–46

Contents lists available at ScienceDirect

Biomaterials

journal homepage: www.elsevier.com/locate/biomaterials

Towards long lasting zirconia-based composites for dental implants. Part I: Innovative synthesis, microstructural characterization and *in vitro* stability

Paola Palmero [a, *], Marta Fornabaio [a], Laura Montanaro [a], Helen Reveron [b], Claude Esnouf [b], Jérôme Chevalier [b, c]

[a] Department of Applied Science and Technology, INSTM R.U. PoliTO, LINCE Lab., Politecnico di Torino, Corso Duca degli Abruzzi, 24, 10129 Torino, Italy
[b] Université de Lyon, INSA de Lyon, MATEIS CNRS UMR5510, 20 Avenue Albert Einstein, F-69621 Villeurbanne Cedex, France
[c] Institut Universitaire de France, 103 bd Saint-Michel, Paris 75005, France

ARTICLE INFO

Article history:
Received 12 September 2014
Accepted 20 January 2015
Available online 14 February 2015

Keywords:
Zirconia
Alumina
Composite
Microstructure
Ageing
Dental implant

ABSTRACT

In order to fulfill the clinical requirements for strong, tough and stable ceramics used in dental applications, we designed and developed innovative zirconia-based composites, in which equiaxial α-Al_2O_3 and elongated $SrAl_{12}O_{19}$ phases are dispersed in a ceria-stabilized zirconia matrix. The composite powders were prepared by an innovative surface coating route, in which commercial zirconia powders were coated by inorganic precursors of the second phases, which crystallize on the zirconia particles surface under proper thermal treatment. Samples containing four different ceria contents (in the range 10.0–11.5 mol%) were prepared by carefully tailoring the amount of the cerium precursor during the elaboration process. Slip cast green bodies were sintered at 1450 °C for 1 h, leading to fully dense materials. Characterization of composites by SEM and TEM analyses showed highly homogeneous microstructures with an even distribution of both equiaxial and elongated-shape grains inside a very fine zirconia matrix.

Ce content plays a major role on aging kinetics, and should be carefully controlled: sample with 10 mol % of ceria were transformable, whereas above 10.5 mol% there is negligible or no transformation during autoclave treatment.

Thus, in this paper we show the potential of the innovative surface coating route, which allows a perfect tailoring of the microstructural, morphological and compositional features of the composites; moreover, its processing costs and environmental impacts are limited, which is beneficial for further scale-up and real use in the biomedical field.

1. Introduction

The excellent mechanical properties of zirconia-based materials combined with their superior aesthetics and biocompatibility characteristics have enlarged, in the last years, their application in the dental field. Particularly, the high strength (>1200 MPa) [1] exhibited by yttria-stabilized zirconia ceramics (Y-TZP) allows them withstanding intermittent forces that arise throughout mastication, thus becoming very interesting materials in prosthetic dentistry. Nowadays, fully dense, translucent yttria-stabilized zirconia ceramics can be processed with fine grains size (0.3 μm), thus meeting esthetic and mechanical requirements [2]. However, the tetragonal (*t*) to monoclinic (*m*) transformation specific of (meta) stabilized zirconia, which is responsible of these extraordinary properties, can also induce a negative phenomenon known as Low Temperature Degradation (LTD), or aging [3]. It consists in a slow transformation of *t*-zirconia to the *m* phase (without any applied stress) in a wide temperature range, typically from room temperature up to around 400 °C, thus including the temperature used for steam sterilization (~140 °C) and the human body temperature (37 °C) [4,5]. Possible consequences are loss of strength and generation of micro-cracks [6].

* Corresponding author. DISAT, Politecnico di Torino, Corso Duca degli Abruzzi, 24, 10129 Torino, Italy. Tel.: +39 011 0904678; fax: +39 011 0904624.
E-mail address: paola.palmero@polito.it (P. Palmero).

http://dx.doi.org/10.1016/j.biomaterials.2015.01.018
0142-9612/

This phenomenon has been well investigated by the orthopedic community since 2001, when a large series of failures of Y-TZP femoral heads was reported [7]. Although the manufacturing process of orthopedic zirconia femoral heads is significantly different from that of dental zirconia, some studies have recently focused on LTD in the dental field [8–13]. Cattani-Lorente et al. [8] and Kohorst et al. [10] observed the reduction of mechanical properties of Y-TZP dental ceramics after LTD. Chevalier et al. [11] evaluated novel porous zirconia dental implants and reported their aging sensitivity. Kim et al. [12] described the influence of different surface treatments on LTD behavior of dental zirconia. Finally, Denry et al. [13] reported that some forms of zirconia are susceptible to aging and that processing conditions can play a critical role in the LTD behavior. Therefore, as well as for orthopedic applications, current research is now focusing on alternative zirconia-based materials to Y-TZP, especially for implants for which the translucency is less important but for which a perfect stability at long durations must be insured in contact with body fluid. Beside the composites in the alumina-zirconia systems [14–17], ceria-stabilized zirconia (Ce-TZP) seems a promising candidate due to its reduced susceptibility to aging and its excellent fracture toughness [18,19]. However, these attractive properties of Ce-TZP are countervailed by its low strength (about 500 MPa [19]) that still prevents its use in biomedical applications. Hence, it is essential to move to composite systems in which the presence of a well-distributed second phase is widely recognized to enhance mechanical properties. Fracture toughness of about 9.8 MPa$\sqrt{m}$ and a mean strength of 950 MPa was reported by Nawa et al. [20,21] for Ce-TZP-based composites containing 30 vol% of Al_2O_3. Higher fracture toughness (about 15 MPa$\sqrt{m}$) and comparable strength (900 MPa) were recently reported by Apel et al. for 10Ce-TZP/$MgAl_2O_4$ composite [22]. Both these systems, characterized by an inter/intra-granular nano-structure, highlight the necessity to carefully tailor and refine the microstructure in order to fulfill the requirements for biomedical ceramics. Since the microstructure is significantly affected by the process conditions (such as powder synthesis and sintering), a deeper understanding of the relationship between microstructure and processing is a key issue to predict mechanical properties.

Among the several elaboration techniques to process zirconia-based composite powders, the most common are the traditional powder milling and mixing method and the co-precipitation route [23–25]. The former, a simple and fast procedure, often yields to materials with severe limitations for what concerns the final phase purity and microstructural homogeneity. On the other hand, co-precipitation route makes it possible to overcome such limitations, but implies expensive chemical precursors and the whole process is much more complex to manage. Recently, a novel processing route has been developed to produce composite powders via surface coating technique [26–28]. Starting from a commercial powder, its surface is coated (or graft) by precursors of the second phase, which crystallizes on the surface of the parent material under proper thermal treatment. The close mixing between the matrix ceramic particles and the precursor is realized at nano/atomic level, assuring an excellent distribution of the second phase in the composite material [28].

In this context, the European project named *LongLife* "Advanced multi-functional zirconia ceramics for long-lasting implants" (7th Framework Program) aims at developing new multi-functional zirconia-based ceramics having a perfect reliability and a lifetime longer than 60 years. To reach this goal, efforts should focus on the improvement of the zirconia stability in the presence of water, while maintaining high toughness and strength. In this paper the strategy of *LongLife* towards strong, tough and stable zirconia-based materials is presented implying *i)* the design of innovative ultra-fine composite structures and *ii)* the use of a new approach named *nano-powder engineering*. Such approach allows a perfect tailoring of the compositional and microstructural features in the developed materials. This is the objective of the Part I of the work, aimed at developing materials designed for dental applications. A comprehensive set of mechanical properties of the developed materials in terms of Vickers hardness, flexural strength and fracture toughness will be reported in Part II, finally showing the potential use of these composites as dental ceramics. Concerning the composite design, we chose Ce-TZP as composite matrix, due to its reduced susceptibility to aging as respect to Y-TZP, and two kinds of second phases characterized by different morphologies: equiaxed and elongated. The role of well-dispersed, fine equiaxed particles is to refine the Ce-TZP microstructure by a *pinning* effect exerted on the zirconia grain boundaries during the sintering cycle. Although refining microstructure increases strength, hardness and wear resistance [29,30], it inevitably decreases the efficiency of the phase transformation toughening [31]. In order to obtain high transformability under stress even with very fine-grained structures, in the present study the ceria content in the composite materials is carefully tailored. In addition, the formation of elongated second-phase particles is promoted, with the aim of further increasing the toughness by additional bridging/crack-deflection mechanisms [32,33]. Precisely, on the ground of the previous scientific literature [15,32–35] α-Al_2O_3 and strontium hexa-aluminate, $SrAl_{12}O_{19}$, were selected as second-phases and added to the Ce-TZP matrix. A preliminary investigation on the biocompatibility of this composite powder showed already promising results in terms of bacterial adhesion, as reported by Karygianni et al. [36], further supporting its employment in the biomedical field.

Fig. 1 shows a schematic strength-toughness relationship for many Y-TZP and Ce-TZP-based materials, according to literature data [1,19–22,30,32,33,37]. It is striking the lack of materials able to meet all the requirements for dental implants (i.e. perfect stability *in vivo*, very high strength and fracture toughness) thus clarifying the objective of *LongLife*, depicted in the same Figure.

The "Longlife composites" are not a new family of zirconia based composites since some studies on (almost) similar compositions are already present in literature [32,34]. However, the innovation and objective of this work is the development of such composites through an innovative surface coating method, simple but very effective in assuring a perfect control of all the microstructural and compositional features of the composite structures. Other surface-

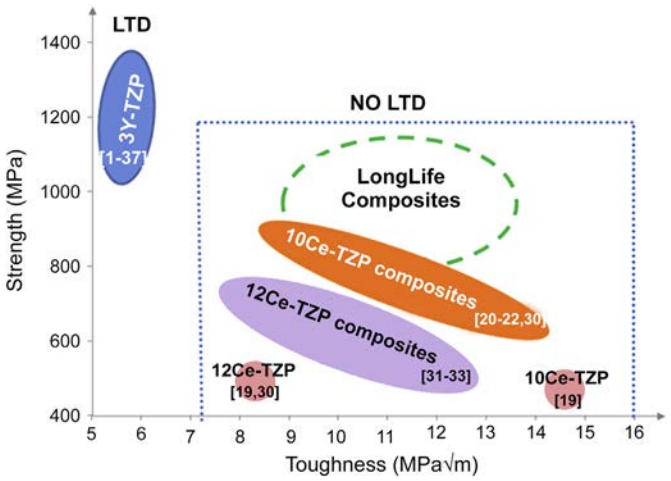

Fig. 1. Relationship strength-toughness for several zirconia-based materials. In green, the objective of LongLife towards LTD-free, strong and tough composites.

coating methods were previously reported in literature by Schehl et al. [26] and Yuan et al. [27], but all using organic media to process the composite powders. On the opposite, our method developed in the last years for alumina-based composites [28] and applied in this study – for the first time – to zirconia-based multi-phase composites, implies the use of only inorganic precursors and aqueous media. In this way, processing costs and environmental impacts of the surface-coating methods can be limited. The process, recently described in an Italian Patent application (TO2014A000145), seems well qualified to be employed, after proper scaling-up, in the industrial manufacturing processes.

2. Materials and methods

2.1. Elaboration of the composite powder

A commercial 10 mol% ceria-stabilized zirconia powder (supplied by Daiichi Kigenso Kagaku Kogio Co. LTD, Japan, referred to as 10Ce-TZP) was employed as raw material to develop composite powders having the following composition: 84 vol% ZrO_2 – 8 vol% Al_2O_3 – 8 vol% $SrAl_{12}O_{19}$ (referred to as ZA_8Sr_8). The starting 10Ce-TZP powder is characterized by a specific surface area of 14.3 m^2/g and an average particle size (by laser diffraction method) of 0.5–1 μm [38]. $Al(NO_3)_3{\cdot}9H_2O$ (>98% purity, Sigma–Aldrich) and $Sr(NO_3)_2$ (>99.0% purity, Sigma–Aldrich) were used as aluminum and strontium precursors, respectively.

In order to modify and tailor the ceria content in the powders, ammonium cerium nitrate ($(NH_4)_2[Ce(NO_3)_6]$, ≥98.5% purity, Sigma–Aldrich) was used as cerium precursor.

First, the zirconia powder was dispersed in distilled water at a solid loading of 8 vol% by ball milling for about 15 h. A pH of 3 was reached by adding diluted hydrochloric acid and this value was maintained all over the process. Zirconia spheres (2.0 mm in diamater, Tosoh Corporation) were selected as milling media since they exhibit high crushing strength and wear resistance [39]. They were used in a weight ratio of 1:10 with respect to the powder. In order to avoid product contamination, zirconia grinding media were periodically replaced. The particle size distribution was determined by using laser-granulometry (Fristch Analysette 22).

The nitrates were then dissolved in distilled water, until clear solutions were obtained. Zirconia to aluminum nitrate weight ratio of 1:0.838 and zirconia to strontium nitrate weight ratio of 1:0.018 were used. In addition, zirconia to cerium nitrate weight ratios of 1:0.02, 1:0.04 and 1:0.06 were employed to obtain 10.5, 11.0 and 11.5 mol%, respectively, of ceria in the zirconia phase. The cerium salt concentration was determined by considering a CeO_2 amount of 10 mol% already present in the raw zirconia powder, as declared by the supplier, and assuming its complete diffusion inside the zirconia lattice during thermal treatments [27].

The nitrate solutions were drop-wise added to the dispersed zirconia slurry; the modified suspension was kept under magnetic stirring for 2 h to assure homogeneity and finally spray-dried. In order to clarify the ceria molar content in the final composites, powders are referred to as ZA_8Sr_8-Ce10, ZA_8Sr_8-Ce10.5, ZA_8Sr_8-Ce11 and ZA_8Sr_8-Ce11.5, being the former composite the only one in which no extra-cerium was added during synthesis.

The as-spray dried powders were submitted to Thermogravimetric and Differential Thermal Analyses (TG-DTA, Netzsch STA 409C) carried out up to 1400 °C (heating and cooling rate of 10 °C/min, under static air).

On the basis of TG-DTA curves, the doped powders were pre-treated at 600 °C for 1 h at the heating rate of 10 °C/min with the aim of inducing the decomposition of the by-products. In addition, a second pre-treatment was carried out in the 900–1450 °C temperature range to induce the crystallization of the second phases on the zirconia particle surface.

The crystalline phases were analyzed by XRD diffraction (Philips PW 1710) with a Cu K_α anticathode in the 10–70° range in 2 theta (a step size of 0.05° and a time for step of 5 s).

2.2. Forming and sintering

Green bodies were prepared by slip casting, which requires the preparation of stable suspensions with suitable solid loading. For this reason, aqueous suspensions of the pre-treated composite powders at a solid loading of 26 vol% were prepared and dispersed by ball-milling for about 30 h. In order to increase the powder dispersibility and to yield stable suspensions, 3 wt% (as respect to the powder weight) of a commercial dispersant (Duramax D-3005) was added. The evolution of the particle size distribution within the dispersion time was determined by laser-granulometry. Green bodies were obtained by casting the dispersed slurries into pure alumina porous molds followed by a drying step into a humidity-controlled chamber for about 1 week. Debinding was carried at 600 °C for 1 h (heating and cooling rate of 5 °C/min).

The densification behavior was investigated by dilatometric analyses (Netzsch 402E) by heating up to 1500 °C, for 1 h. Tests were carried out at three different heating rates, being precisely 2, 5 and 10 °C/min.

Materials were obtained by pressureless sintering in the temperature range 1400–1450 °C, for different dwell times (1–2 h). As a comparison, 10Ce-TZP and 3Y-TZP reference materials were also prepared. Slip cast 10Ce-TZP was sintered in the 1450 °C–1500 °C for 1–3 h, whereas granules of 3Y-TZP were cold isostatic pressed and sintered at 1450 °C for 2 h, following the standard procedure reported in literature for this material [2].

2.3. Characterizations

The green and fired densities were evaluated by mass-geometric measurements and Archimedes method and referred to the materials theoretical density (TD), calculated by the rule of mixtures for composite systems (values of 6.19, 5.82, 3.99 and 4.02 g/cm^3 for tetragonal and monoclinic ZrO_2, α-Al_2O_3 and $SrAl_{12}O_{19}$ were respectively used).

The phase composition was investigated by XRD, and the monoclinic volume content (V_m) was determined by applying the Toraya's equation [40].

The microstructures were analyzed by means of Scanning Electron Microscopy (SEM Zeiss SUPRA VP55) and Field Emission Scanning Electron Microscopy (FESEM Hitachi S4000) on polished and thermally etched specimens. The mean grain sizes of matrix and second phases were determined by image analysis (Scandium Soft imaging system software). In addition, high-resolution Transmission Electron Microscopy (HRTEM JOEL 2010 F) equipped for EDX nanoprobe analyses and X-rays mapping was used on selected composition (ZA_8Sr_8-Ce11). Selected Area Diffraction (SAED) and Fast Fourier Transform (FFT) of the HRTEM images from DigitalMicrograph™ software were used to index the crystalline phases.

Finally, the sintered materials were submitted to preliminary hydrothermal aging tests, with the aim of investigating the role of the ceria content on the *in-vitro* stability. The tests were performed in autoclave (Fisher Bioblock Scientific) at 134 °C under 2 bar pressure. After controlled period of time, XRD analysis was carried out in order to evaluate the content of the monoclinic phase during the aging test.

3. Results and discussion

3.1. Elaboration of the composite powders

Ball milling was effective in dispersing the starting zirconia agglomerates to the desired particle size: the mean diameter of the volume distribution (d_{50}) decreased from 1.1 to 0.5 μm as reported in Table 1. In Fig. 2, a SEM micrograph of the dispersed powder is depicted, showing a small agglomerate, of about 0.5 μm, in which primary particles of less than 100 nm can be easily recognized.

Nitrates aqueous solutions were added to such dispersed powder and the suspension was spray dried. This is a key point of the process since a fine dispersion of the raw powder and a fast drying step assure a homogeneous coating of zirconia particles by the precursors of the second-phases. As a consequence, a homogeneous distribution of the second phases in the final composite materials can be achieved [41]. In order to avoid aluminum hydroxide precipitation [42], the pH of the suspension was kept stable at a value of 3. In Fig. 3 the TG-DTA curves of the spray-dried ZA_8Sr_8-Ce11 powder are depicted. The TG curve shows a mass loss of about 30%, due to the decomposition of the synthesis by-products (mainly the nitrates), which was almost accomplished at about 500 °C. Accordingly, after spray drying, all powders were calcined at 600 °C for 1 h, in order to assure the precursors decomposition. The DTA curve shows a broad, exothermic peak at about 1200 °C, imputable to both α-Al_2O_3 and $SrAl_{12}O_{19}$ crystallization. Precisely, as reported by Douy et al. [43], it is supposed that alumina crystallizes into the γ-Al_2O_3 phase at about 950 °C,

Table 1
Diameters (d_{10}, d_{50} and d_{90}) of the particle size distribution before and after ball-milling (BM) of 10Ce-TZP and ZA_8Sr_8-Ce11 powder.

	d_{10} (μm)	d_{50} (μm)	d_{90} (μm)
10Ce-TZP before BM	0.5	1.1	2.3
10Ce-TZP after BM	n.d.[a]	0.5	0.8
ZA_8Sr_8-Ce11 before BM	11	42	255
ZA_8Sr_8-Ce11 after BM	n.d.[a]	0.5	0.9

[a] n.d. means below the instrumental limit (<0.31 μm).

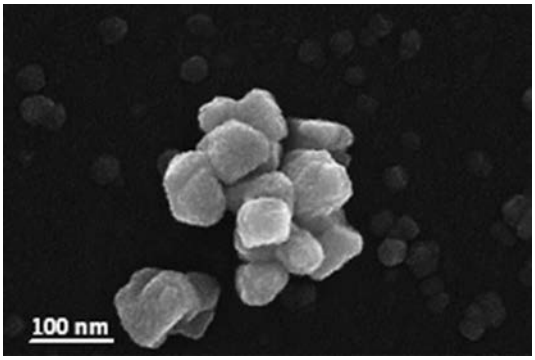

Fig. 2. SEM micrograph of the dispersed 10Ce-TZP powder.

transforming into the high temperature phases (α-Al_2O_3 and $SrAl_{12}O_{19}$) at about 1200 °C. The TG-DTA curves of the composites having different ceria contents are very similar to those of Fig. 3 and so they are not included.

XRD patterns of ZA_8Sr_8-Ce11 powders thermally treated in the range 600–1450 °C are shown in Fig. 4. In agreement with DTA and Douy's results, at lower temperature (up to 900 °C) only monoclinic (ICDD no. 74-0815) and tetragonal (ICDD no. 82-1398) zirconia phases were detected (spectra a–c Fig. 4). At higher temperature, precisely 1050 and 1150 °C (spectra d–e Fig. 4), diffracted peaks ascribed to a transition alumina phase were expected. However, they were not detected since their intensity was too low compared to ZrO_2 phase. In fact, it should be mentioned that the intensity of the diffraction peaks is related to the crystallization degree and the type of element, namely to the Z-number. By increasing the temperature up to 1450 °C (spectrum f Fig. 4) diffracted peaks imputable to α-Al_2O_3 (ICDD no. 46-1212) and $SrAl_{12}O_{19}$ (ICDD no. 80-1195) phases were observed, being higher the crystallization degree. Nevertheless, their intensity was very low with respect to the intensity peaks of ZrO_2 phase. By XRD diffractograms, we could also observe a clear influence of the thermal treatment on the monoclinic volume fraction (V_m). In fact, in the as-spray dried materials, V_m was about 75% and it progressively decreased by increasing the calcination temperatures, reaching the minimum value (about 4%) after calcination at 1150 °C (see V_m values in Fig. 4). This trend was expected on the ground of the ceria-zirconia phase diagram [3] and can be also imputed to an increasing stabilization effect of ceria

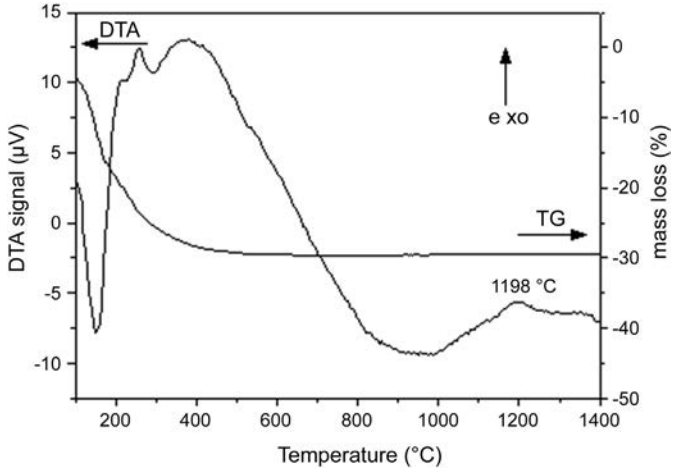

Fig. 3. TG-DTA curves of the spray-dried ZA_8Sr_8-Ce11 powder.

inside the zirconia lattice, being the diffusion of the cerium oxide promoted by the higher temperature treatments [27].

3.2. Processing and sintering

On the ground of the previous results, all powders were calcined at 1150 °C, for 30 min. All thermally treated powders showed a good dispersibility with a strong decrease of the agglomerate size after 30 h of ball milling, independently on the ceria content. The diameter corresponding to 10, 50 and 90% of the volume distribution (d_{10}, d_{50} and d_{90}, respectively) of ZA_8Sr_8-Ce11 (as an example) are reported in Table 1. After ball milling, the values of d_{50} and d_{90} decreased from 42 to 255 to 0.5 and 0.9 μm, respectively.

The slip cast green bodies had a similar density, in the range 2.8–2.9 g/cm^3.

In order to define the best sintering cycle and investigate the effect of the heating rate on the composite densification behavior, dilatometric curves were recorded on ZA_8Sr_8-Ce11 sintered up to 1500 °C for 1 h at the heating rate of 2, 5 and 10 °C/min (Fig. 5). After sintering, all the materials reached full densification: precisely, ZA_8Sr_8-Ce11 sintered at 2 °C/min and 5 °C/min reached a density >99.9%TD, whereas the material heated at 10 °C/min reached a slightly lower value (99.0%TD). Other differences in the densification behavior can be ascribed to the heating rate (Fig. 5(a)): the materials sintered at the two lower heating rates had almost superimposable dilatometric curves, whereas the one sintered at 10 °C/min was displaced at higher temperatures (of about 20 °C–50 °C), as already observed in literature for other oxide ceramic materials [44]. This can be better observed by the derivative curves (Fig. 5(b)), showing the onset sintering temperature at about 1070 °C for the 2 and 5 °C/min sintered samples and at about 1090 °C for the 10 °C/min sintered one. Moreover, two major inflection points can be observed by the derivatives curves: the former, in the range 1150 °–1185 °C, can be reasonably imputed to the crystallization of both second phases, thus confirming the DTA data. The latter inflection point can be instead ascribed to the temperature corresponding to the maximum densification rate of the composites. Precisely, this temperature increases by increasing the heating rate, being respectively 1265 °C, 1280 °C and 1320 °C for the 2, 5 and 10 °C/min-sintered materials. These results make it possible to select the best heating rate (5 °C/min), which was used in the following sintering processes. After sintering at 1450 °C for 1 h, at the heating and cooling rate of 5 °C/min, all the composite materials reached full densification. Reference 3Y-TZP sintered at 1450 °C for 2 h also reached full densification, whereas 10Ce-TZP after sintering at 1450 °C for 1 h yielded a final density of about 97% TD. Full densification of this material was obtained after increasing the sintering temperature to 1500 °C, for 3 h.

3.3. Sintered materials characterization

XRD analyses performed on the as-sintered materials showed the presence of tetragonal and monoclinic zirconia phases as well as of α-Al_2O_3 and $SrAl_{12}O_{19}$ phases. In addition, V_m decreased as the ceria content increased: V_m was 7, 5, 3 and 1 vol% for ZA_8Sr_8-Ce10, ZA_8Sr_8-Ce10.5, ZA_8Sr_8-Ce11 and ZA_8Sr_8-Ce11.5, respectively.

These results also suggest that the surface coating process was successful in producing composites having the desired composition, but also in tailoring the ceria amount inside the zirconia grains. The lower the ceria content during synthesis, the higher the monoclinic fraction after sintering.

SEM-FESEM observations (Fig. 6) showed completely homogeneous and dense microstructures with an even distribution of all the phases inside the composite materials, whatever the ceria content. The second phase particles had the desired morphology,

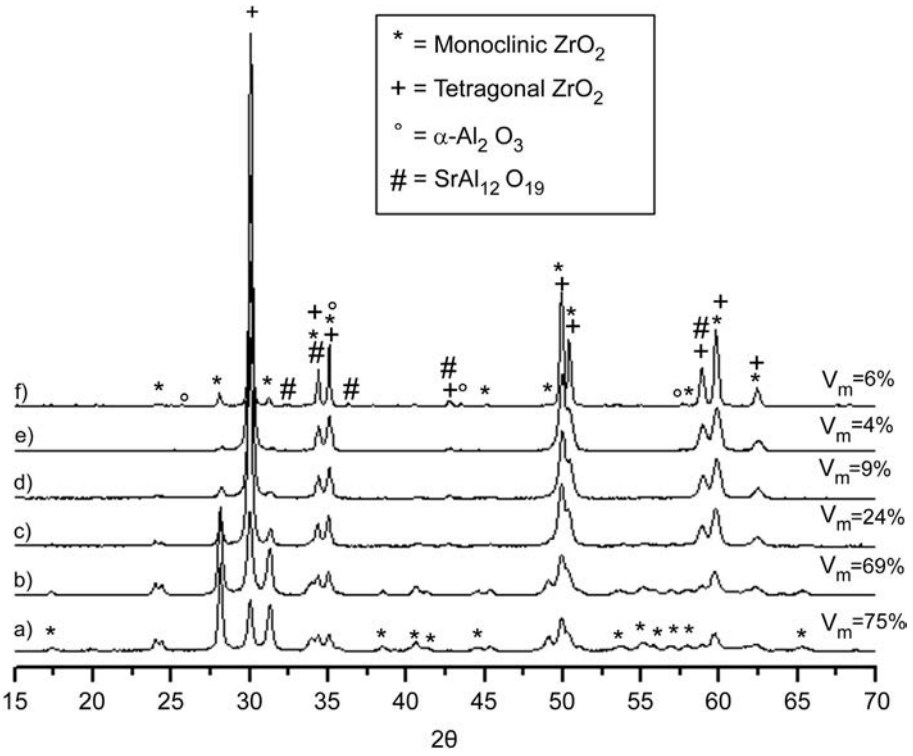

Fig. 4. XRD patterns of ZA_8Sr_8-Ce11 powders: a) spray-dried and calcined at b) 600 °C for 1 h, c) 900 °C for 1 h, d) 1050 °C for 30 min, e) 1150 °C for 30 min, f) 1450 °C for 1 h. The monoclinic volume fraction (Vm) is also reported.

both rounded (α-Al_2O_3 phase) and elongated ($SrAl_{12}O_{19}$ phase). Although the second phases were mainly located in inter-granular positions, it was possible to observe a minor fraction of ultra-fine alumina grains within the larger zirconia particles.

Fig. 6(a) and (b) refer to ZA_8Sr_8-Ce11, but the same microstructural features can be observed in samples containing different ceria amounts. By image analysis, an average particle size of 0.6 ± 0.2 μm and of 0.3 ± 0.1 μm for zirconia and alumina grains, respectively, were determined. The strontium hexa-aluminate grains were characterized by mean length of 0.6 ± 0.2 μm and aspect ratio of 5 ± 2. The well-dispersed alumina particles exerted an effective *pinning* on zirconia grain boundaries, leading to zirconia grains almost three-four times smaller than in reference Ce-TZP sintered at 1500 °C for 3 h, necessary to reach full densification. In fact, as shown in Fig. 6(c), pure monolithic 10Ce-TZP showed a coarsened microstructure with a mean grain size of 2.4 μm, in agreement with previous literature data [19]. For sake of comparison, also a FESEM micrograph of sintered 3Y-TZP is depicted in Fig. 6(d) showing a very homogeneous and dense microstructure with zirconia grains of about 0.4 μm in size. Since the microstructural features of 10Ce-TZP were completely different from those of the composite materials, it cannot be considered as a proper reference and it will not be further discussed in this work. On the contrary, physical and mechanical properties of the

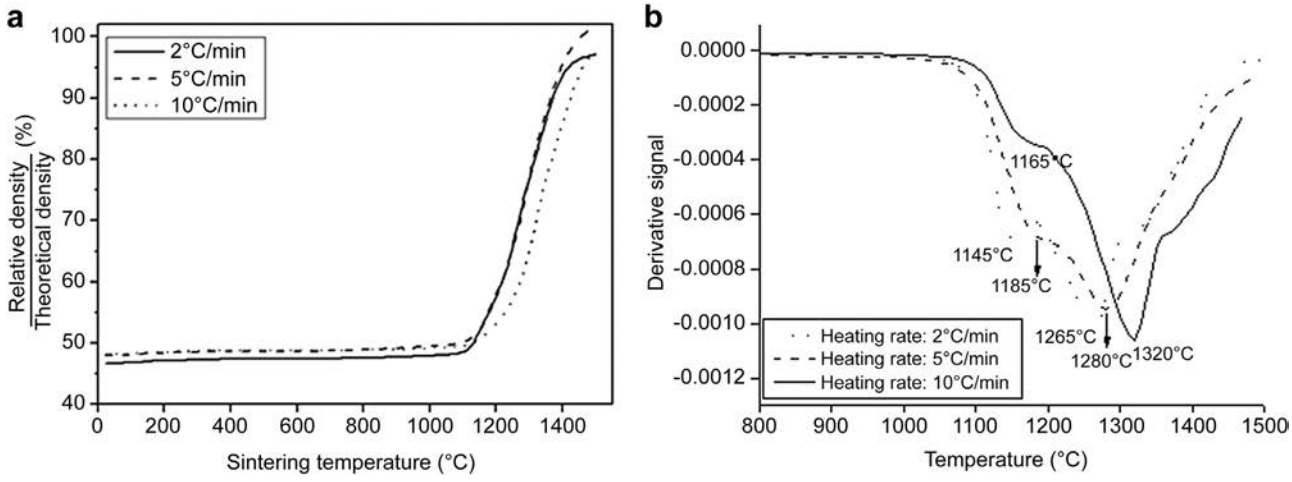

Fig. 5. Densification (a) and derivative - in the range 800 °–1500 °C (b) curves of ZA_8Sr_8-Ce11 sintered at 1500 °C for 1 h at different heating rates.

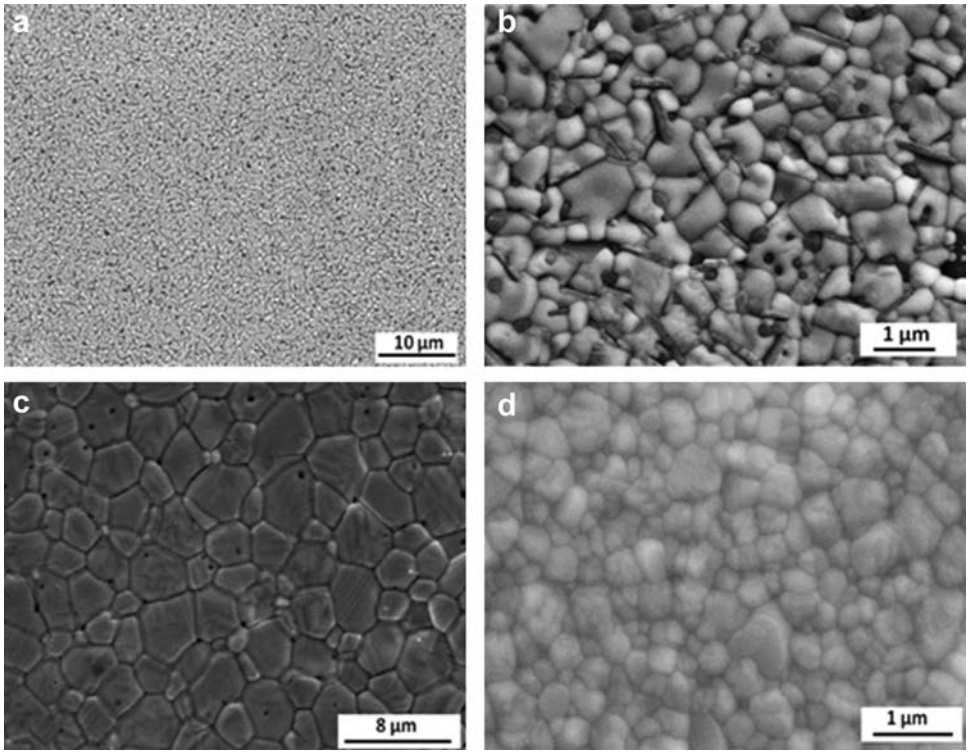

Fig. 6. FESEM micrographs of the microstructure of ZA_8Sr_8-Ce11 sintered at 1450 °C for 1 h (bright zirconia grains, dark round-shaped α-Al_2O_3 grains and dark elongated-shaped $SrAl_{12}O_{19}$ grains) (a, b); FESEM micrographs of reference 10Ce-TZP sintered at 1500 °C for 3 h (c) and 3Y-TZP sintered at 1450 °C for 2 h (d).

composites will be compared to those of 3Y-TZP, at present, the benchmark ceramic material for dental applications (mechanical properties will be discussed in Part II).

A deeper insight into the microstructure of a sintered sample is given in Fig. 7 by HR-TEM analysis, where brighter regular-shape, darker elongated- and equiaxial-shape grains can be easily recognized. To define the chemical composition of the particles having different morphologies and phase contrast, EDX nanoprobe was focused on the grains referred to as A, B and C in Fig. 7. The corresponding atomic compositions are shown in the Table enclosed to Fig. 7: even if a low zirconium amount was observed both in A and B grains due to a matrix effect, a quite perfect agreement with their nominal compositions was found. In fact, in the point A (dark elongated grain), an atomic Sr:Al ratio of 6:87 (=1:14.5) corroborates, within the instrumental error (thin foil geometry could influence uncontrolled absorption effect), an aluminate phase composition very close to $SrAl_{12}O_{19}$. At the same time, it was confirmed that the dark equiaxial grain (grain B) was pure alumina. Regarding the brighter grain (point C), it is pure zirconia stabilized with ceria: the atomic Zr:Ce ratio of 90:10 showed a zirconia stabilization degree lower than the expected value (Zr:Ce ratio of 90:11) but still within the instrumental error. Since cerium was detected only inside the zirconia grains, TEM analyses confirm its complete diffusion inside the zirconia lattice during thermal treatments, thus corroborating the ability of the applied method in tuning the zirconia stabilization degree. In addition, EDX maps were also performed (Fig. 8) clearly proving *i)* zirconium and cerium in the brighter grains, *ii)* strontium only present inside the elongated grains and *iii)* aluminum in both dark rounded and elongated grains. The phase identification was carried out by exploiting the Fast Fourier Transformation (FFT) from HRTEM micrographs and by comparison with the lattice distance with the

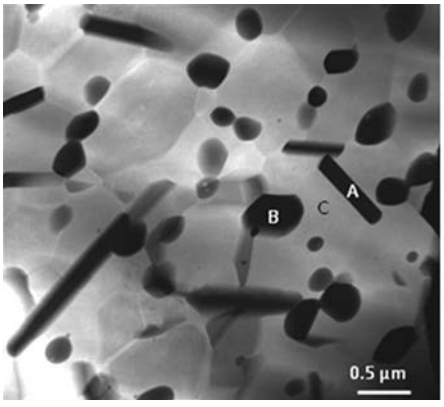

Grain	Chemical composition			
	Zr (at%)	Ce (at%)	Al (at%)	Sr(at%)
A	6	0	87	6
B	6	0	94	0
C	90	10	0	0

Fig. 7. TEM image (left) and chemical composition (at%) on the A, B and C grains (right) of the ZA_8Sr_8-Ce11 sintered sample.

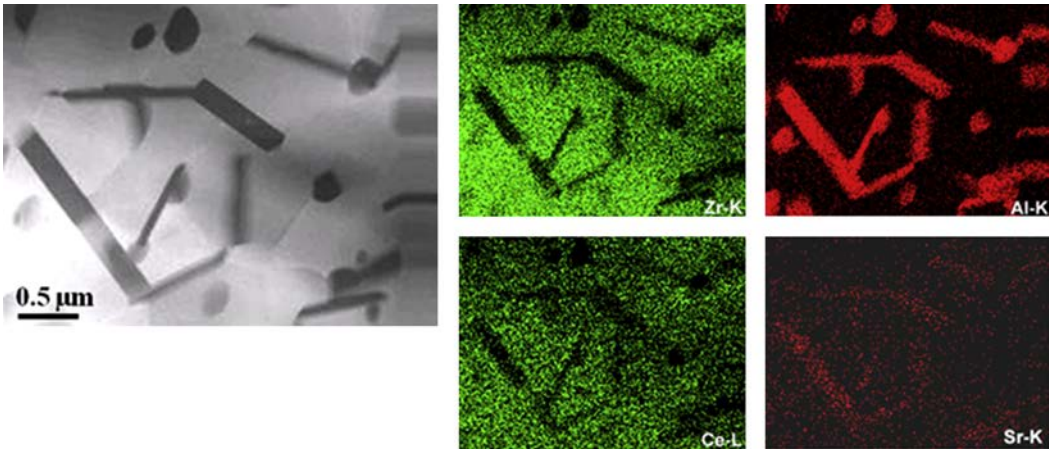

Fig. 8. TEM image and corresponding EDX maps of the ZA_8Sr_8-Ce11 sintered sample.

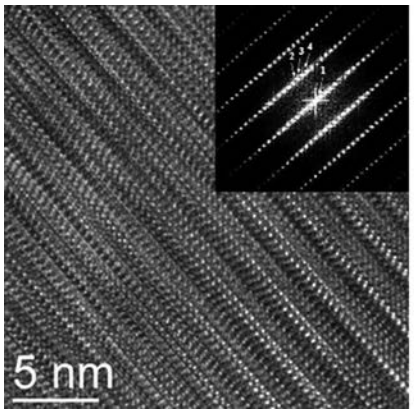

Spot	d_{exp}(nm)	d $SrAl_{12}O_{19}$	{hkl}	Deg. to spot 1	Deg. $SrAl_{12}O_{19}$
1	2.22	2.20	0001	0.0°	0°
2	0.483	0.482	1-100	89.8°	90°
3	0,476	0,471	1-101	77.8°	77.6°
4	0,446	0,442	1-102	66.1°	66.3°

Fig. 9. HRTEM micrograph of a $SrAl_{12}O_{19}$ grain in zone axis [010] (inset to the figure, its FFT) (left) and the corresponding FFT analysis (right).

ICDD files. As an example, in Fig. 9 an HRTEM image and the associated FFT (inset to the figure) of a strontium aluminate grain is reported. According to the lattice distances and respective angles between lattice planes of ICDD file no. 80-1195, the indexation corresponds to the hexagonal $SrAl_{12}O_{19}$ phase. FFT performed on an alumina and a zirconia grain confirm the crystallography of α-Al_2O_3 (ICDD no. 46-1212) and a tetragonal-ZrO_2 (ICDD no. 82-1398) phase, respectively. Finally, by HR-TEM, the interfaces between the

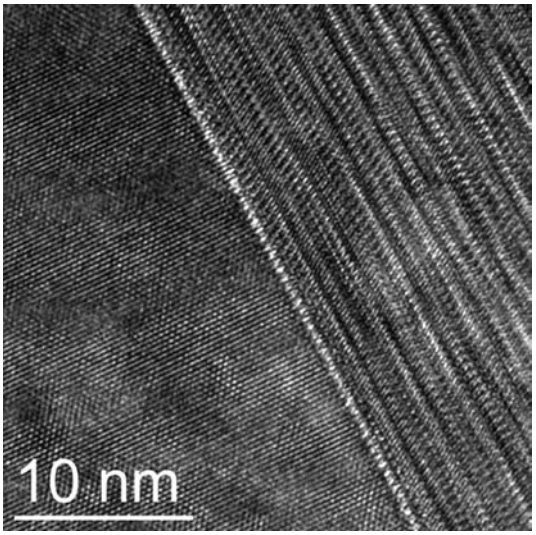

Fig. 10. HRTEM micrograph of the interfacial region between a tetragonal zirconia grain (on the left) and a $SrAl_{12}O_{19}$ elongated grain (on the right).

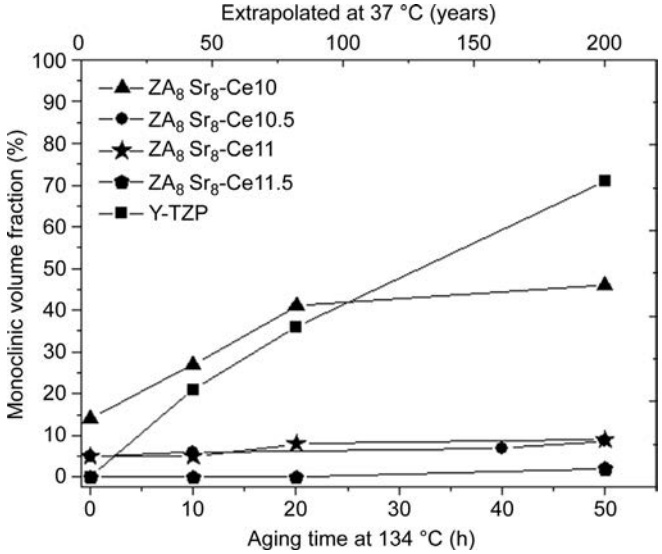

Fig. 11. The monoclinic volume fraction as a function of time during the aging test for several compositions. Results related to as-sintered surfaces.

different phases inside the composite materials were investigated. An example is provided in Fig. 10, showing the interface between a tetragonal zirconia grain (on the left) and a $SrAl_{12}O_{19}$ elongated grain (on the right). We can observe a clean interface, free form glassy or secondary phases. The systematic observation of the interfaces and the FFT carried out on the related grains allowed to evidence the lack of specific crystallographic relationships between the platelets and the zirconia species. In addition, the intrinsic quality of interfaces between different phases seems good, since neither reactional compounds nor nanoscale porosities have been observed at a nanoscale.

Preliminary aging results of the as-sintered samples are reported in Fig. 11. As expected, a high transformation ratio was observed in the 3Y-TZP material: 20 h of aging were enough to reach a monoclinic fraction of 20 vol% and the monoclinic phase increased up to 70 vol% after 50 h. ZA_8Sr_8-Ce10 was the most transformable composite material and the monoclinic volume fraction moved from 15 to 40 vol% after 20 h, then it remained almost stable. Once the *t* to *m* transformation starts, probably due to a water-vapor-mediated mechanism, the tensile stress in the remaining tetragonal zirconia within the deformation bands increases and consequently, the overall compressive stress within the band increases as well. As reported by Sergo et al. [45], this tensile stress is responsible of a cerium reduction from Ce^{4+} to Ce^{3+} that in turn provides a positive feedback for the growth of the bands. However, as the tetragonal grains in the bands decrease, the tensile stress decreases as well, hindering the cerium reduction. This phenomenon could partly explain the plateau of the monoclinic amount and the clear slope change observed in the range of 20–50 h of ageing. However, a deeper investigation is still in progress to confirm the above hypothesis.

For materials with higher cerium amount (10.5–11.5 mol%), a negligible transformation was observed, even after 50 h of treatment. According to the extrapolation proposed by Chevalier et al. [46], 50 h of test would correspond to about 150–200 years *in vivo*: this means that composites containing 10.5 mol% of ceria, or more, fulfill the stability requirements for medical applications.

4. Conclusions

This work describes an innovative design and processing of zirconia-based composites for dental application. The 10 mol% ceria-stabilized zirconia powder was added with both equiaxed (α-Al_2O_3) and elongated ($SrAl_{12}O_{19}$) second phases. Some samples were also added with extra-ceria, with the aim of increasing the ceria amount in the sintered materials up to 11.5 mol%. The composite powders were produced by a simple but reliable surface coating process, in which zirconia powders were coated by inorganic precursors (nitrates) of the second phases, which crystallize on the zirconia particles surface under proper thermal treatment. In this work we demonstrate the effectiveness of the method in the precise and simultaneous tuning of many compositional (i.e. the ceria amount inside the zirconia phase, the stoichiometry and purity of the second phases) and microstructural (i.e. the grain size, morphology and distribution of the phases) features in the final ultra-fine composite structures. The microstructures were fully dense and highly homogeneous with optimal distribution of both second phases inside a very fine zirconia matrix. The fine control of the ceria amount inside zirconia allowed the production of stable materials, at ceria contents equal or higher than 10.5 mol%, as demonstrated by *in vitro* hydrothermal tests. By these results, some of the developed composites fully satisfy the stability requirements for medical applications. However, to have a full evidence of the potential use of these materials in dentistry, the (forthcoming) Part II of this work has to be considered, in which the mechanical properties (fulfilling the International Standard ISO 6872:2008 for dental ceramics) will be presented and discussed.

Acknowledgment

The research leading to these results has been performed within the LONGLIFE project (www.longlife-project.eu) and received funding from the European Community's Seventh Framework Programme (FP7/2007-2013) under grant agreement n° 280741.

The authors would like to acknowledge the CLYM (Centre Lyonnais de Microscopie (http://www.clym.fr) for the access of the JEOL 2010F.

References

[1] Fisher J, Stawarczyk B. Compatibility of machined Ce-TZP/Al_2O_3 nanocomposite and a veneering ceramic. Dent Mater 2007;23:1500–5.
[2] Denry I, Holloway JA. Ceramics for dental applications: a review. Materials 2010;3:351–68.
[3] Chevalier J, Gremillard L, Virkar AV, Clarke DR. The tetragonal-monoclinic transformation in zirconia: lesson learned and future trends. J Am Ceram Soc 2009;92:1901–20.
[4] Lawson S. Environmental degradation of zirconia ceramics. J Eur Ceram Soc 1995;15:485–502.
[5] Lughi V, Sergo V. Low temperature degradation -aging- of zirconia: a critical review of the relevant aspects in dentistry. Dent Mater 2010;26:807–20.
[6] Chevalier J. What future for zirconia as a biomaterial? Biomaterials 2006;27:535–43.
[7] Chevalier J, Gremillard L. Zirconia as a biomaterial, vol. 1. Comprehensive Biomaterials-Elsevier; 2011. p. 95–108.
[8] Cattani-Lorente M, Scherrer SS, Ammann P, Jobin M, Wiskott A. Low temperature degradation of a Y-TZP dental ceramic. Acta Biomater 2011;7:858–65.
[9] Sanon C, Chevalier J, Douillard T, Kohal RJ, Coelho PG, Hjerppe J, et al. Low temperature degradation and reliability of one-piece ceramic oral implants with a porous surface. Dent Mater 2013;29:389–97.
[10] Kohorst P, Borchers L, Strempel J, Stiesch M, Hassel T, Bach FW, et al. Low-temperature degradation of different zirconia ceramics for dental applications. Acta Biomater 2012;8:1213–20.
[11] Chevalier J, Loh J, Gremillard L, Meille S, Adolfson E. Low-temperature degradation in zirconia with a porous surface. Acta Biomater 2011;7:2986–93.
[12] Kim JW, Covel NS, Guess PC, Rekow ED, Zhang Y. Concerns of hydrothermal degradation in AD/CAM zirconia. J Dent Res 2010;89:91–5.
[13] Denry I, Kelly JR. State of the art of zirconia for dental applications. Dent Mater 2008;24:299–307.
[14] De Aza AH, Chevalier J, Fantozzi G, Schehl M, Torrecillas R. Crack growth resistance of alumina, zirconia and zirconia toughened alumina ceramics for joint prostheses. Biomaterials 2002;23:937–45.
[15] Chevalier J, Grandjean S, Kuntz M, Pezzotti G. On the kinetics and impact of tetragonal to monoclinic transformation in an alumina/zirconia composite for arthroplasty applications. Biomaterials 2009;30:5279–82.
[16] Fabbri P, Piconi C, Burresi E, Magnani G, Mazzanti F, Mingazzini C. Lifetime estimation of a zirconia-alumina composite for biomedical applications. Dent Mater 2014;30:138–42.
[17] Kurtz SM, Kocagöz S, Arnholt C, Huet R, Ueno M, Water WL. Advances in zirconia toughened alumina biomaterials for total joint replacement. J Mech Behav Biomed Mater 2014;31:107–16.
[18] Chevalier J, Gremillard L. Ceramics for medical applications: a picture for the next 20 years. J Eur Ceram Soc 2009;29:1245–55.
[19] El Attaoui H, Saàdaoui M, Chevalier J, Fantozzi G. Static and cyclic crack propagation in Ce-TZP ceramics with different amounts of transformation toughening. J Eur Ceram Soc 2007;27:483–6.
[20] Nawa M, Nakamoto S, Sekino T, Niihara K. Tough and strong Ce-TZP/alumina nanocomposites doped with titania. Cer Int 1998;24:497–506.
[21] Nawa M, Bamba N, Sekino T, Niihara K. The effect of TiO_2 addition on strength and toughening in intragranular type 12Ce-TZP/Al_2O_3 nanocomposites. J Eur Ceram Soc 1998;18:209–19.
[22] Apel E, Ritzberger C, Courtois N, Reveron H, Chevalier J, Schweiger M, et al. Introduction to a tough, strong and stable Ce-TZP/$MgAl_2O_4$ composite for biomedical applications. J Eur Ceram Soc 2012;32:2697–703.
[23] Thuan WH, Chen Z, Wang TC, Cheng CH, Kuo PS. Mechanical properties of Al_2O_3/ZrO_2 composites. J Eur Ceram Soc 2002;22:2827–33.
[24] Rafferty A, Alsebaie AM, Olabi AG, Prescott T. Properties of zirconia-toughened-alumina prepared via powder processing and colloidal processing routes. J Colloid Interf S C 2009;329:310–5.
[25] Bhattacharyya S, Pratihar SK, Sinha RK, Behera RC, Ganguly RI. Preparation of alumina-high zirconia microcomposite by combined gel-precipitation. Mater Lett 2002;53:425–31.
[26] Schehl M, Diaz JA, Torrecillas R. Alumina nanocomposites from powder-alkoxide mixtures. Acta Mater 2002;50:1125–39.

[27] Yuan Z, Vleugels J, Van Der Biest O. Synthesis and characterization of CeO_2-coated ZrO_2 powder-based TZP. Mater Lett 2000;46:249–54.
[28] Palmero P, Naglieri V, Chevalier J, Fantozzi G, Montanaro L. Alumina-based nanocomposites obtained by doping with inorganic salt solutions: application to immiscible and reactive systems. J Eur Ceram Soc 2009;29:59–66.
[29] Tanaka K, Tamura J, Kawanabe K, Nawa M, Oka M, Uchida M, et al. Ce-TZP/Al_2O_3 nanocomposite as a bearing material in total joint replacement. J Biomed Mater Res 2002;63:262–7.
[30] Benzaid R, Chevalier J, Saâdaoui M, Fantozzi G, Nawa M, Diaz LA, et al. Fracture toughness, strength and slow crack growth in a ceria stabilized zirconia–alumina nanocomposite for medical applications. Biomaterials 2008;29:3636–41.
[31] Swain MV, Rose LRF. Strength limitations of transformation-toughened zirconia alloys. J Am Ceram Soc 1986;69:511–8.
[32] Cutler RA, Lindemann JM, Ulvensøen JH, Lange HI. Damage-resistant SrO-doped Ce-TZP/Al_20_3 composites. Mater Des 1994;15:123–33.
[33] Burger W, Richter HG. High strength and toughness alumina matrix composites by transformation toughening and "in situ" platelets reinformcement (ZPTA)-the new generation of bioceramics. Key Eng Mat 2011;192:545–8.
[34] Kern F. A comparison of microstructure and mechanical properties of 12Ce-TZP reinforced with alumina and in situ formed strontium- or lanthanum-hexaaluminate precipitates. J Eur Ceram Soc 2014;34:413–23.
[35] Cutler RA, Mayhew RJ, Prettyman KM, Virkar AV. High toughness Ce-TZP/Al_2O_3 ceramics with improved hardness and strength. J Am Ceram Soc 1991;74:179–86.
[36] Karygianni L, Jähnig A, Schienle S, Bernsmann F, Adolfsson E, Kohal RJ, et al. Initial bacterial adhesion on different yttria-stabilized tetragonal zirconia implant surfaces in vitro. Materials 2013;6:5659–74.
[37] Chevalier J, Saâdaoui M, Olagnon C, Fantozzi G. Double-torsion testing a 3Y-TZP ceramic. Cer Int 1996;22:171–7.
[38] http://www.dkkk.co.jp/english.
[39] http://www.tosoh.com/our-products/advanced-materials/zirconia-grinding–dispersion-media.
[40] Toraya H, Yoshimura M, Somiya S. Calibration curve for quantitative analysis of the monoclinic-tetragonal ZrO_2 system by X-ray diffraction. J Amer Ceram Soc 1984;67:C119–21.
[41] Naglieri V, Joly-Pottuz L, Chevalier J, Lombardi M, Montanaro L. Follow-up of zirconia crystallization on a surface modified alumina powder. J Eur Ceram Soc 2010;30:3377–87.
[42] Bahn CB, Kasza KE, Shack WJ, Natesan K, Klein P. Evaluation of precipitates used in strainer head loss testing: part III. Long-term aluminum hydroxide precipitation tests in borated water. Nucl Eng Des 2011;241:1914–25.
[43] Douy A, Capron M. Crystallization of spray-dried amorphous precursors in the SrO-Al_2O_3 system: a DSC study. J Eur Ceram Soc 2003;23:2075–81.
[44] Montanaro L, Palmero P, Lombardi M, Esnouf C, Chevalier J, Cardinal S. Thermal analyses applied to ceramic nanopowders: from synthesis to sintering. A review on transition alumina powder-based materials. J Therm Anal Calorim 2013;112:437–45.
[45] Sergo V, Clarke DR. Deformation bands in ceria-stabilized tetragonal zirconia/alumina: II. Stress-induced aging at room temperature. J Amer Ceram Soc 1995;78:641–4.
[46] Chevalier J, Gremillard L, Deville S. Low-temperature degradation of zirconia and implications for biomedical implants. Ann Rev Mat Res 2007;37:1–32.